THE ASTROPHYSICAL JOURNAL, 207:484–501, 1976 July 15

SHOCK-DRIVEN IMPLOSION OF INTERSTELLAR GAS CLOUDS AND STAR FORMATION

PAUL R. WOODWARD
National Radio Astronomy Observatory*
Received 1975 May 9; revised 1975 August 28

ABSTRACT

Two-dimensional hydrodynamical calculations are presented to demonstrate a mechanism of star formation which, within the context of the spiral density wave theory, can explain the narrowness of the spiral arms of galaxies delineated by the classic spiral tracers—the bright, young stars and their associated H II regions. The implosion of a standard interstellar cloud has been followed numerically after it encounters a shock in the intercloud medium. Parameters have been chosen to represent a cloud flowing into a spiral arm which is delineated by a shock in the interstellar gas. Although this work is motivated by spiral wave theory, the results should also be indicative of the evolution of a cloud struck, for example, by a supernova shock.

The asymmetrical surface pressure distribution tends to flatten the cloud into a general pancake shape, so that gravitational collapse of the cloud as a whole cannot occur. The low sound speed and rapid cooling within the cloud cause the implosion to be completed before the cloud is accelerated appreciably in the direction of relative flow of the shocked intercloud gas. The compressed cloud gas is therefore subjected to a very large effective surface pressure (ram pressure), which makes gravitational collapse of subregions of the cloud possible. Gravitationally bound subregions are formed from the action of the Rayleigh-Taylor instability of the front cloud surface. Where the Kelvin-Helmholtz instability also has a chance to act, dense tongues of compressed material are formed which project outward from the front of the cloud.

Densities sufficient to produce observable CO emission are attained in the thin shell at the front of the cloud. If observed CO sources are such thin shells rather than spheres, their mass estimates then fall in a range which is theoretically tractable. Ordered gas motions in such shells give rise to supersonic broadening of CO line profiles. In contrast to spherical collapse models for CO sources, this model implies that only about 5 percent of the visible material ends up in stellar form. A time for shock-initiated star formation of order 10^7 years, as previously estimated observationally, is obtained from the calculation.

Subject headings: hydrodynamics — nebulae: general — shock waves — stars: formation

I. INTRODUCTION

The work described here constitutes a detailed calculation of a process suggested years ago for star formation in spiral galaxies (Roberts 1969; Shu *et al.* 1972). This process—shock-driven implosion of interstellar clouds—is envisaged within the context of the spiral density-wave theory of galactic structure (Lin, Yuan, and Shu 1969). Observations of the older populations of the stellar disks of spiral galaxies—that is, observations of the mass distributions rather than the light distributions of these galaxies—reveal relatively little spiral structure. Hence in treating the dynamics of these stellar disks only a linear theory of spiral waves is required. Such a treatment yields very broad spiral arms, where the stellar surface density varies with azimuth, θ, as $\sin 2\theta$.

Observations of the young populations of the stellar disks of spiral galaxies, which comprise only small fractions of the masses of the disks, reveal very striking, thin spiral arms. These young stars must have formed from the interstellar gas within times quite short compared to the orbital periods in these galaxies. Therefore, it is natural to attempt an explanation of the narrow spiral arms they form by pointing to a nonlinear response of the interstellar gas to the linear spiral wave of the stellar disk. Such a response is possible because of the low value of the sound speed of the gas compared to the velocity dispersion of the stars. It has been shown that, for moderately large amplitudes of the stellar spiral wave, shocks develop in the interstellar gas which trace the spiral pattern (Roberts 1969; Shu *et al.* 1972; Shu, Milione, and Roberts 1973; Woodward 1975). If star formation can be triggered by these shocks, then the narrow spiral arms delineated by the youngest stars can be explained within the context of the spiral wave theory.

a) Purpose

The present work focuses upon the process by which a spiral-wave shock may trigger star formation. In obtaining sufficient final density for the gravitational collapse of a stellar mass of gas, it is helpful to begin before the shock with an interstellar gas cloud. To collect so large a mass of gas into a cloud volume

* Operated by Associated Universities, Inc., under contract with the National Science Foundation.

starting only with intercloud density, or some average interstellar density, requires a time comparable to the period of galactic rotation, particularly if a one-dimensional compression along magnetic field lines is necessary. The star formation process triggered by a spiral-wave shock must occur much more rapidly if the thin spiral traced by that shock is to be reflected by the new stars produced behind it. Therefore, in specifying our initial conditions we are driven to the two-phase model of the interstellar medium (Zel'dovich and Pikel'ner 1969; Field, Goldsmith, and Habing 1969; Spitzer and Scott 1969), and to Spitzer's standard cloud in particular (Spitzer 1968). We will start with a cloud 25 percent more massive than standard, which we shall refer to loosely as standard. In the low pressure of the interarm region this cloud has a radius of 15 pc, a density of 1.5 H atoms cm^{-3}, a temperature of 140 K, and a mass of 500 $M_\odot$.

The aim of the present work is to produce a massive, compressed clump of interstellar gas by subjecting a standard interstellar cloud to a fairly strong shock in the intercloud medium surrounding it. The resulting gas clump must be sufficiently dense that its self-gravity will overwhelm all other forces and cause it to collapse. It must also be sufficiently massive that the result of this gravitational collapse can be presumed to be a star. The protostellar gas concentration is to be formed by a combination of two forces—the pressure of the shocked intercloud gas, which is now higher than that within the cloud, and the dynamic pressure from the motion of that shocked gas relative to the cloud. The purpose of the detailed calculation reported here is to assess the effects upon the cloud implosion of the asymmetry of the effective intercloud pressure distribution and of the instability of the cloud surface during the implosion.

b) Method

It is worthwhile to complete this Introduction with some remarks about the numerical method used in this work. In order to appreciate why this work was pursued in the way it was and why the presentation takes the form it does, it is necessary to understand the demands which are placed upon the numerical method by the nature of the problem. First, the asymmetry of the cloud implosion forces us to carry out a two-dimensional treatment. Second, the large density contrast between the cloud and intercloud gas makes a straightforward numerical treatment, even on a very fine mesh, impossible. The high density and low temperature in the cloud imply that the shock which will be driven into it will travel much more slowly than the original shock in the intercloud gas. Therefore, the intercloud gas near the cloud will be shocked and will acquire a high velocity relative to the cloud before the cloud itself can be accelerated very much. Hence vortices will eventually develop in the shocked intercloud gas behind the cloud. To describe this motion in our simulation we must use an Eulerian grid.

The high density and low temperature in the cloud place another restriction on the calculation. They imply that radiative cooling will be very rapid in the gas behind the cloud shock. Considering the shock to include the thin cooling region behind the viscous shock itself, we see that the cloud shock will cause the density to increase by an enormous factor (in the calculation it is of order 100). Behind this shock moving into the cloud a very dense, thin shell of gas will form. In an Eulerian treatment, the position of this shell would have to be constantly interpolated as the shell moved inward. The interpolation errors would cause a diffusion of the mass, momentum, and energy of the shell to occur. Therefore, in an Eulerian treatment the shell would spread out, and decent accuracy in the calculation would be impossible to maintain. To avoid this difficulty, the cloud must be described by a two-dimensional Lagrangian grid. Such a description results in a very rapid and accurate calculation for the cloud evolution.

It is only possible to perform a meaningful simulation of this problem because of the existence of the hydrodynamics code CEL. This code has been developed over many years at the Lawrence Livermore Laboratory by W. F. Noh and his co-workers. The main features of the numerical method used by CEL have been described by Noh (1964). The principal advantage of CEL is that it allows different regions of a single problem to be described by Eulerian or Lagrangian meshes. The Lagrangian mesh is allowed to move relative to the Eulerian mesh. The correct motion of the Lagrangian region is ensured by an extremely complicated, and time-consuming, calculation of pressures which act on the Lagrangian boundary. The boundary calculation is outlined by Noh (1964); only two general features need to be mentioned here. First, completely free slip along the boundary is permitted. This feature is essential in treating instabilities of the boundary accurately. Second, a minimum ratio of Lagrangian to Eulerian zone sizes must normally be maintained at the boundary in order to allow a reasonable calculation of the boundary pressures. If a certain zone size is required by the problem in the Lagrangian region, this second feature of the boundary treatment may not permit a coarse, and therefore rapid, calculation in the Eulerian region.

The problem at hand makes great demands upon the calculation at the Lagrangian-Eulerian boundary (the cloud boundary). This boundary is subject to both the Kelvin-Helmholtz and Rayleigh-Taylor instabilities, and we have every reason at the outset of the computation to expect their role in the cloud evolution to be of critical importance (we shall see later that indeed this is the case). Because the CEL code defines the position of the boundary very well (it is *not* uncertain, for instance, by an Eulerian zone width) and also allows free slip along it, we can calculate the development of these boundary instabilities. We can treat the modes of larger wavelength, which in our case are the more important modes, if we provide enough zones along the boundary. For this purpose a wavelength must be divided into at least

10 zones, and an accurate treatment should require about twice this many.

The treatment of the boundary instabilities sets the most stringent zoning requirements, and the computation presented here is zoned just about as coarsely as is possible to achieve a *meaningful* result. This involves a cloud with 90 zones along the boundary (which goes halfway around the cloud, because of cylindrical symmetry), 60 of which are spaced evenly along the more important front half. At any particular time in the calculation, grid points in the unshocked region of the cloud are useless, except just ahead of the shock. Therefore, when the Lagrangian grid was rezoned, an attempt was always made to distribute the available grid points to give maximum accuracy and minimum artificial diffusion. For this reason the accuracy of the calculation varies greatly over the cloud and can only be displayed by showing the Lagrangian grid used. In the figures, therefore, this grid is always shown. In each case it is shown at its worst, just before rezoning. At this point the grid has become most distorted and yields the least accurate computational results.

The above requirements on the numerical method not only affect the figure format in this paper; they also dictate the entire system of approach we must take. To describe the instabilities of the cloud surface we used a Lagrangian grid of over 3600 zones. The Eulerian grid used to match this contained over 18,000 zones in a 96- by 188-zone format. Part of this huge grid was needed to insure that the presence of reflective and flow-in-flow-out boundaries should not affect the calculation in the region near the cloud. Mostly, however, this grid size was needed for the accurate treatment of the cloud boundary instabilities. Although the CEL code is very fast (about 3000 grid points per second), over 5 hours of CDC 7600 time was required to carry the one run presented here to completion. A comparable amount of machine time and a tremendous amount of time at the Teletype was needed to perform the many Lagrangian grid rezonings (machine time required to remap a region increases as the square of the number of grid points, so that rezoning is relatively expensive). As a result, only a single case could be thoroughly treated. It was therefore necessary that a case be chosen for calculation which a maximum number of astrophysicists would consider reasonable. This case was by no means the most favorable for eventual star formation. It is necessary to learn from the results of that single calculation what the most important processes are and how they compete or cooperate to produce the computed cloud evolution. Using this understanding together with scaling laws which can be applied to the results, we must make informed extrapolations to cases other than that computed in order to draw conclusions of more general astrophysical importance.

II. STATEMENT OF THE PROBLEM

a) Two-Phase Model

In this work the interstellar gas is considered as consisting of two phases in pressure equilibrium—cool, dense clouds, and a hot, tenuous intercloud medium. The intercloud gas has temperatures near 10,000 K and densities which normally range between about 0.015 and 0.2 H atoms cm^{-3}. The clouds have temperatures which range between about 140 K and 20 K and densities which range between about 1.5 and 100 atoms cm^{-3}. These phases represent the two thermally stable states, at a given pressure, for which heating of the gas by cosmic rays is balanced by radiative cooling. That two such states are possible, at least within a range of pressures from p_{min} to p_{max} (see Fig. 1), is due to the different dependence upon density of the heating and cooling rates (cf. Field, Goldsmith, and Habing 1969). The curve of heating and cooling balance is shown in Fig. 1.

The flow of such a composite gas in a spiral density wave was computed by Shu *et al.* (1972). As the composite gas flows from a spiral arm into the interarm region in a spiral wave of moderately large amplitude, it is decompressed, and it expands until the pressure drops to p_{min}, below which only the intercloud phase is thermally stable. At this point cloud material begins to evaporate, and the pressure can drop further only when no clouds remain (the time scale for cloud evaporation is relatively short). Thus p_{min} is a likely value for the pressure before a spiral shock. If that shock is moderately strong, it will raise the pressure above p_{max}, so that only the cloud phase is thermally stable. Cloud material will then condense downstream from the shock until the pressure drops to p_{max}. In order to avoid the complication of this condensation in the calculations presented here, while retaining a fairly strong shock, the postshock pressure was chosen to be p_{max}.

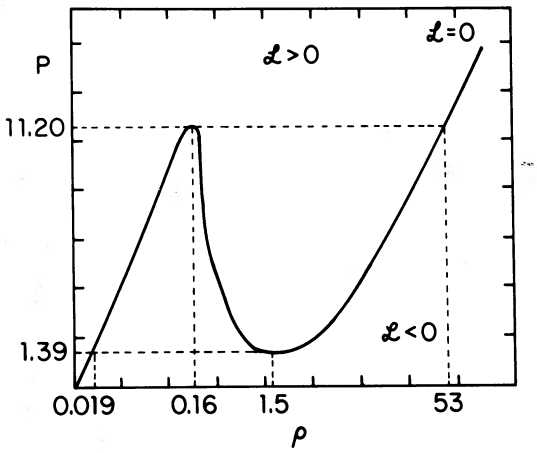

FIG. 1.—The curve of heating and cooling balance is plotted for a cosmic ray ionization rate $\zeta = 1.2 \times 10^{-15}\ s^{-1}$. $\mathscr{L}$ is the net cooling rate. Special values of density and pressure are indicated, although the scales of the plot are logarithmic. A system of units is used in which length, velocity, and density are measured in parsecs, km s^{-1}, and H atoms cm^{-3}, respectively.

b) *Equation of State*

In the numerical calculation discussed below, heating and cooling were approximated as occurring immediately in the cloud phase and as not occurring at all in the intercloud phase. The equation of state which was used is displayed in Figure 2. In the cloud gas the pressure was assumed to depend upon density only. A simple relationship was chosen which follows the curve of heating and cooling balance between temperatures of 140 K and 26 K. Below 26 K and above 140 K the gas was treated as isothermal and isobaric, respectively. The realm of high temperature is unimportant because it is never reached; it is only necessary that the equation of state used here introduce no thermal instabilities near 140 K. This approximation of short cooling time scales for the cloud phase is excellent. It describes a gas which is very easily compressed and in which very large changes of density and temperature can occur over very short distances. Such a gas presents no insurmountable difficulties for a Lagrangian calculation but is nearly impossible to represent in an Eulerian treatment.

The intercloud gas was represented by a polytropic equation of state with index 5/3. This corresponds to the approximation of long cooling time scales in this gas phase. One-dimensional calculations indicate that the cooling time behind the spiral shock is about 10^5 years and that this shock is nearly isothermal (see, for instance, Shu *et al.* 1972). Therefore, the numerical calculation without cooling in the intercloud gas represents the postshock kinetic pressure properly, by construction, but it greatly underestimates the dynamic pressure of the postshock gas upon the cloud surface. The effects of this misrepresentation upon the results of the calculation are discussed later. Here it suffices to say that the lack of cooling in the intercloud gas makes eventual star formation considerably more difficult to achieve.

The polytropic representation of the intercloud gas was made from necessity. The shocked intercloud gas must flow around the cloud with perfectly free slip, and it must be free to develop vortices. The first requirement is critical for the proper treatment of surface instabilities, while the second is essential in computing the implosion of the back surface of the cloud. These requirements demand an Eulerian representation for the intercloud gas. However, if the spiral shock is nearly isothermal, the cloud motion relative to the gas behind that shock is supersonic, and a bow shock must form. An Eulerian difference scheme necessarily has so much numerical diffusion that it cannot allow the huge temperature and density gradients which occur in the region of cooling and phase transition behind such a bow shock.

An advantage of the composite equation of state described above is that it permits an accurate computation of the cloud evolution. Essential to this accuracy is the coupled Eulerian-Lagrangian feature of the hydrodynamics code which was used (CEL, described in detail by Noh 1964). Physical arguments will later be made which imply that allowing cooling in the intercloud gas would be favorable for star formation. Some approximate treatment of that cooling would demand a much more difficult assessment of the cumulative effect of significant numerical errors upon the computational results.

c) *Initial Parameters*

In the computed example discussed below, the post–spiral-shock pressure is set to p_{max}, the maximum pressure for which an intercloud gas is thermally stable in the two-phase model. The pre–spiral-shock

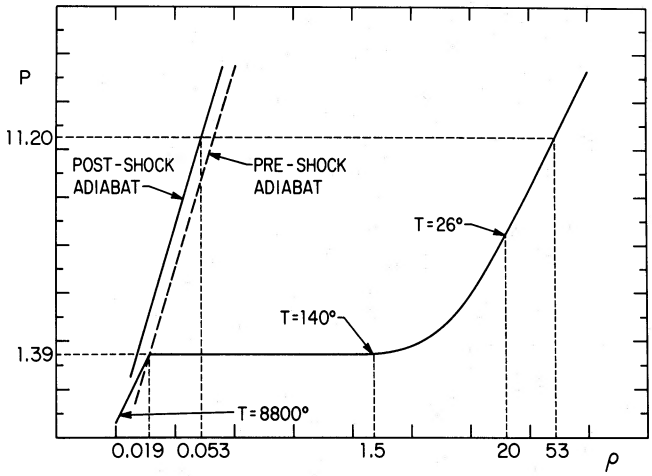

FIG. 2.—The composite equation of state used in the numerical computation. For the cloud material, heating and cooling are assumed immediate, and the pressure is represented as a function of density only. The cloud equation of state is made up of four segments, the first two of which were never reached during the computations: an isothermal, intercloud segment at 8800 K, an isobaric segment at p_{min}, a cubic segment in which the temperature decreases from 140 K to 26 K, and another isothermal segment at 26 K for densities above 20 atoms cm^{-3}. The intercloud gas is a polytrope with index $\gamma = 5/3$. The adiabat corresponding to the pre–spiral-shock state (at p_{min}) is shown as a dashed line, while that corresponding to the post–spiral-shock state (at p_{max}) is shown as a solid line. Special values of density and pressure are indicated, although the scales of the plot are logarithmic.

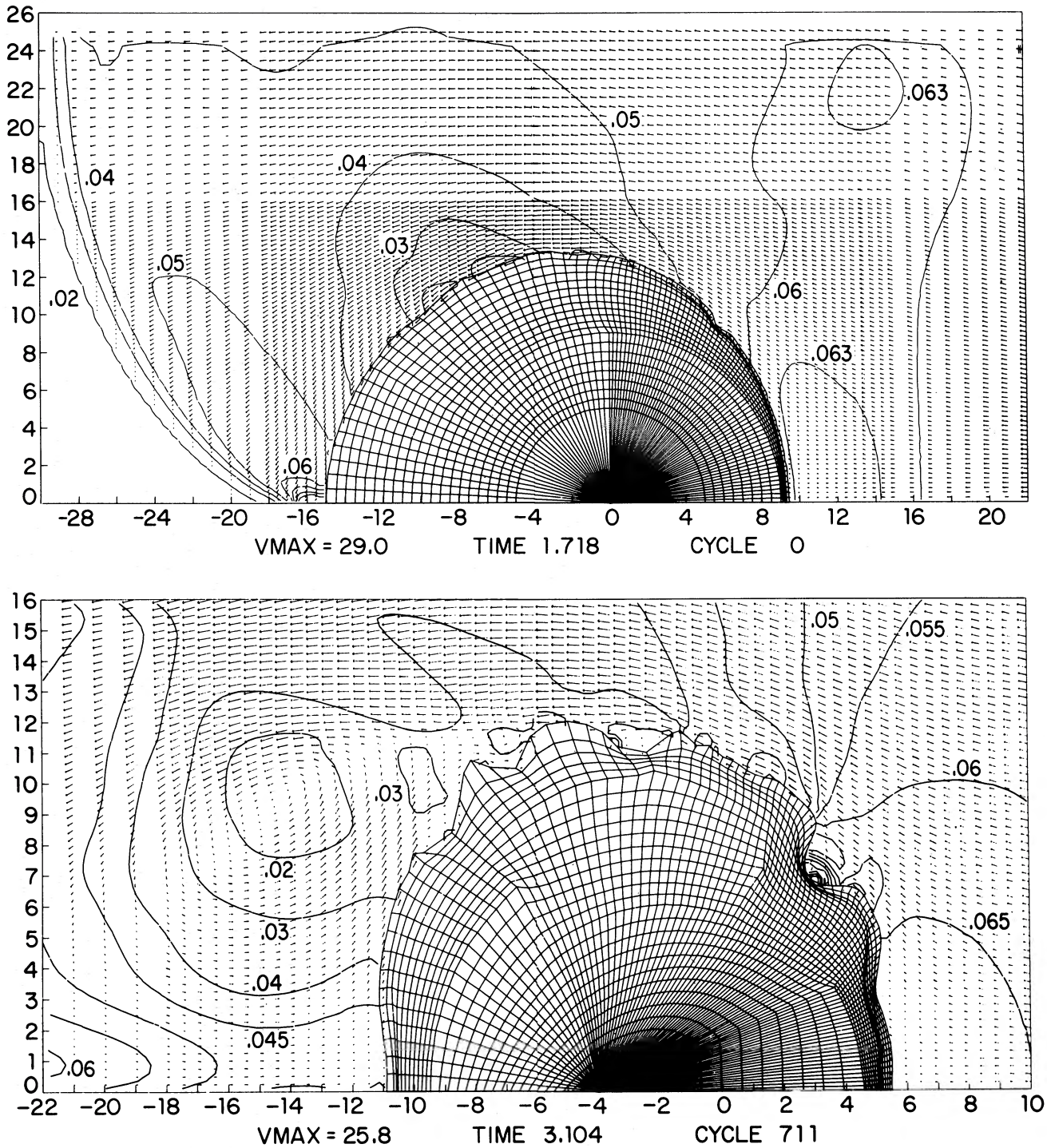

FIG. 3 (*top*).—View of the originally spherical cloud at $t = 1.7$ (time unit = 10^6 years). The spiral shock has struck the front cloud surface at $t = 0.2$. By now it has just passed completely over the cloud. A reflected shock is seen at the back of the cloud, and along the sides ripples are growing from the Kelvin-Helmholtz instability. Cycle numbers for this problem begin at -800 for $t = 0$, distance is measured in parsecs, and VMAX gives the length, in km s^{-1}, of the longest velocity vector shown. Further details of the display format are given in the text. Representative densities within the thin shell of compressed cloud material follow, in units of H atoms cm^{-3} and with (r, z) coordinates of the approximate locations: 90 (0, 8.7), 80 (5, 8.25), 55 (8, 7.75), 50 (9, 5), 37 (10, 4.75), 17 (12.5, 2), 5.6 (10, -10), 3.4 (6.5, -13), 1.5 (0, -15).

FIG. 4 (*bottom*).—The cloud is shown at $t = 3.1$, when it has been compressed longitudinally to half its original dimension. Behind the cloud a large vortex can be seen, and along its side Kelvin-Helmholtz modes of large scale have become nonlinear. This Kelvin-Helmholtz amplification is responsible for the large-amplitude perturbations of the front surface away from the symmetry axis. The Rayleigh-Taylor instability will now cause these to grow very rapidly. A shock moving into the cloud near its surface can be located along the front and back by a sudden compression of the Lagrangian grid lines. Interior to this shock the grid has been redrawn but, of course, the gas there is still undisturbed. Shell densities and their locations are as follows: 100 (0, 5.4), 95 (1.5, 5.4), 74 (3.25, 5.2), 74 (5.75, 5), 60 (7, 2.75), 43 (8.75, 2.9), 30 (10.25, 1), 15 (8.25, -8.75), 30 (3, -11), 35 (0, -10.75).

pressure is set to p_{min}, the minimum pressure for which a cloud gas is stable. A system of units is used throughout in which length is measured in parsecs, velocity in km s^{-1}, and density in H atoms cm^{-3}. In these units the pre- and post-spiral-shock pressures are 1.38 and 11.2, so that the pressure jump is about a factor of 8. It is reasonable that such a shock would be produced by a spiral density wave, and the work of Shu *et al.* (1972) has shown that this may be the most interesting representative case. The numerical computation is so difficult that a parameter study is out of the question.

Initially, the spherical interstellar cloud has a radius of 15 pc, a density of 1.5 atoms cm^{-3}, a temperature of 140 K, and a total mass of 500 $M_\odot$. It is in pressure equilibrium with a surrounding intercloud gas with a temperature of about 11,000 K and a density of 0.019 atoms cm^{-3}. The cloud's self-gravity is negligible, and it is confined by the pressure of the intercloud gas. A shock in the intercloud gas is fed in at the right-hand end of the computational grid. The shocked intercloud gas has a velocity of 18 km s^{-1} and a sound speed of about 20 km s^{-1}. After this shock has passed over the cloud, the motion of the cloud through the shocked intercloud gas is subsonic.

d) Format for Figures

The computer-generated figures conform to a fairly uniform format. Distances along the axes are marked off in parsecs, with origin at the initial location of the cloud center. Each figure is labeled by a problem time in millions of years and a cycle number referred to an initial cycle number −800 at time zero. In Figures 3, 4, and 7, velocity vectors are plotted at every Eulerian grid point along every other vertical grid line. In Figures 5, 6, and 8, velocity vectors are plotted at every grid point in the Eulerian region. The length in km s^{-1} of the longest velocity vector shown is given as VMAX in the label of each figure. Also in the Eulerian region isodensity contours are plotted which are labeled in units of H atoms cm^{-3}. The Lagrangian grid representing the cloud is shown in all but Figure 8, and the cloud shock can usually be located by a compression of that grid. Interior to the shock the cloud density is uniform; but, because of rezoning, the Lagrangian grid is not. The Lagrangian grid does not represent the density; instead it indicates the accuracy of the computation in the various regions of the cloud.

In all but the final figures in the time sequence shown, the region of compressed cloud material forms a very thin shell at the cloud surface. Because it is impossible to display the variation of density over this region on the figure, representative values of the density at various points along this boundary region are given in the figure legends. A rough idea of the density in this shell is conveyed by the extent to which the cloud surface has been pushed in from its original position. More important to observe at these earlier times is the shape of the cloud boundary and the shape and number of Lagrangian zones which are used to describe any individual features it possesses. The zoning conveys the accuracy of the calculation and indicates which features of the computed cloud are to be believed and which are to be taken as merely indicative of how such a cloud would "really" look. The fully developed Kelvin-Helmholtz modes along the back top of the cloud in the later figures clearly fall in this latter category.

III. SUMMARY OF RESULTS

a) Computed Evolution

The evolution of the computer simulation is described below. Occasional references to problem times are made in units of 10^6 years. The cloud is at first compressed by a shock whose strength and speed decrease with increasing distance from the symmetry axis. The large tangential slip velocity along the sides of the cloud causes ripples of that part of the cloud surface to be amplified by the Kelvin-Helmholtz instability. These growing ripples get a head start toward the front side of the cloud where the slip first occurs, and later ripples also grow around the side of the cloud and down toward the back. At the back of the cloud the slip vanishes and there is no amplification from this instability.

When it passes over the cloud, the spiral shock bends as the postshock gas rushes down behind the cloud. At $t = 1.7$ (Fig. 3), the various sections of the shock at different azimuths meet at the back of the cloud. The downward motion of the shocked gas is then arrested by a reflected shock. Behind this new shock directly at the back of the cloud very high pressures are developed transiently ($p \approx 26.5 \approx 2p_{max}$). These pressures force the back of the cloud inward and strengthen the spiral shock behind the cloud. The result is that the spiral shock is straightened out downstream from the cloud and that a shock propagates in from the back of the cloud somewhat less rapidly than the shock coming in from the front. The inward flow of intercloud gas at the back of the cloud and the upward propagation of the reflected spiral shock (it is eventually weakened to a pressure wave) result in the formation of a vortex behind the cloud. The pressure of the intercloud gas behind the cloud and its motion due to the vortex then continue to drive the back of the cloud inward.

By about $t = 3$ (Fig. 4), the front of the cloud becomes sufficiently flattened in its general shape that the first original side ripples created by the Kelvin-Helmholtz instability can be amplified by the Rayleigh-Taylor instability. These ripples constitute a large-amplitude perturbation of the cloud surface and are therefore amplified relatively rapidly. They develop into long tongues of dense gas whose shapes, insofar as they can be represented by a Lagrangian mesh, are characteristic of nonlinear Rayleigh-Taylor instability. Nearer the symmetry axis the cloud surface also buckles due to Rayleigh-Taylor instability, but there has been no prior development due to Kelvin-Helmholtz instability in this region.

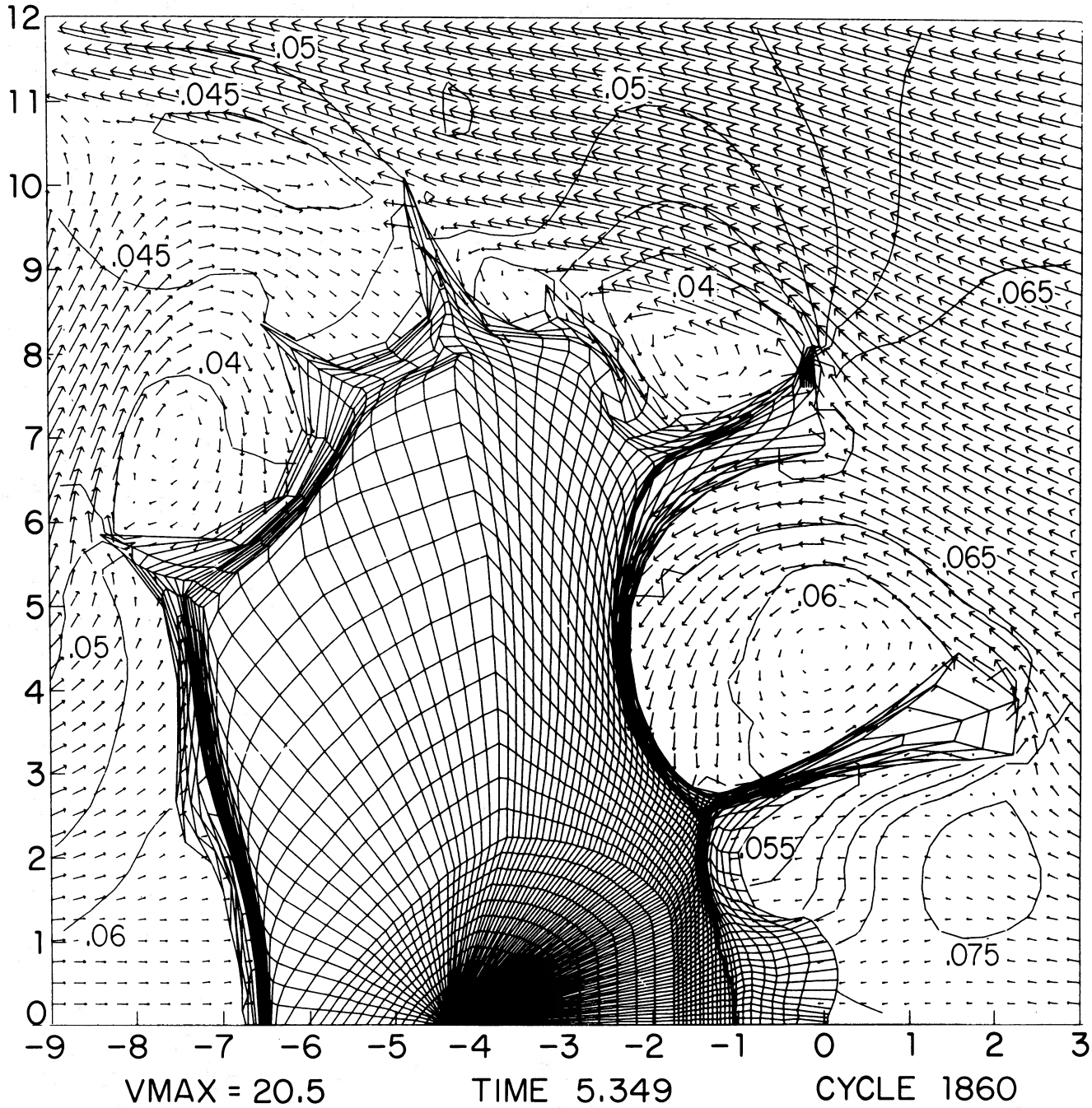

FIG. 5.—A close-up view of the cloud at $t = 5.35$. Velocity vectors are plotted at every Eulerian mesh point. The Rayleigh-Taylor instability of the front surface has caused previous Kelvin-Helmholtz modes to grow into long, dense tongues of compressed material. These contain a substantial fraction of the gas swept up by the cloud shock. Near the symmetry axis the instability has become nonlinear. It consists principally of two modes, one half the wavelength of the other. The clump of compressed gas centered on the axis contains 25 $M_\odot$ of material. Shell densities and their locations are as follows: 280 (0, −0.5), 110 (0.75, −0.2), 60 (2, −1.2), 70 (3.75, 1.75), 50 (4.5, −2.35), 70 (7, −0.25), 50 (7.75, −0.25), 45 (7.5, −2), 20 (6.25, −6.25), 30 (2.5, −7.25), 55 (0, −6.6).

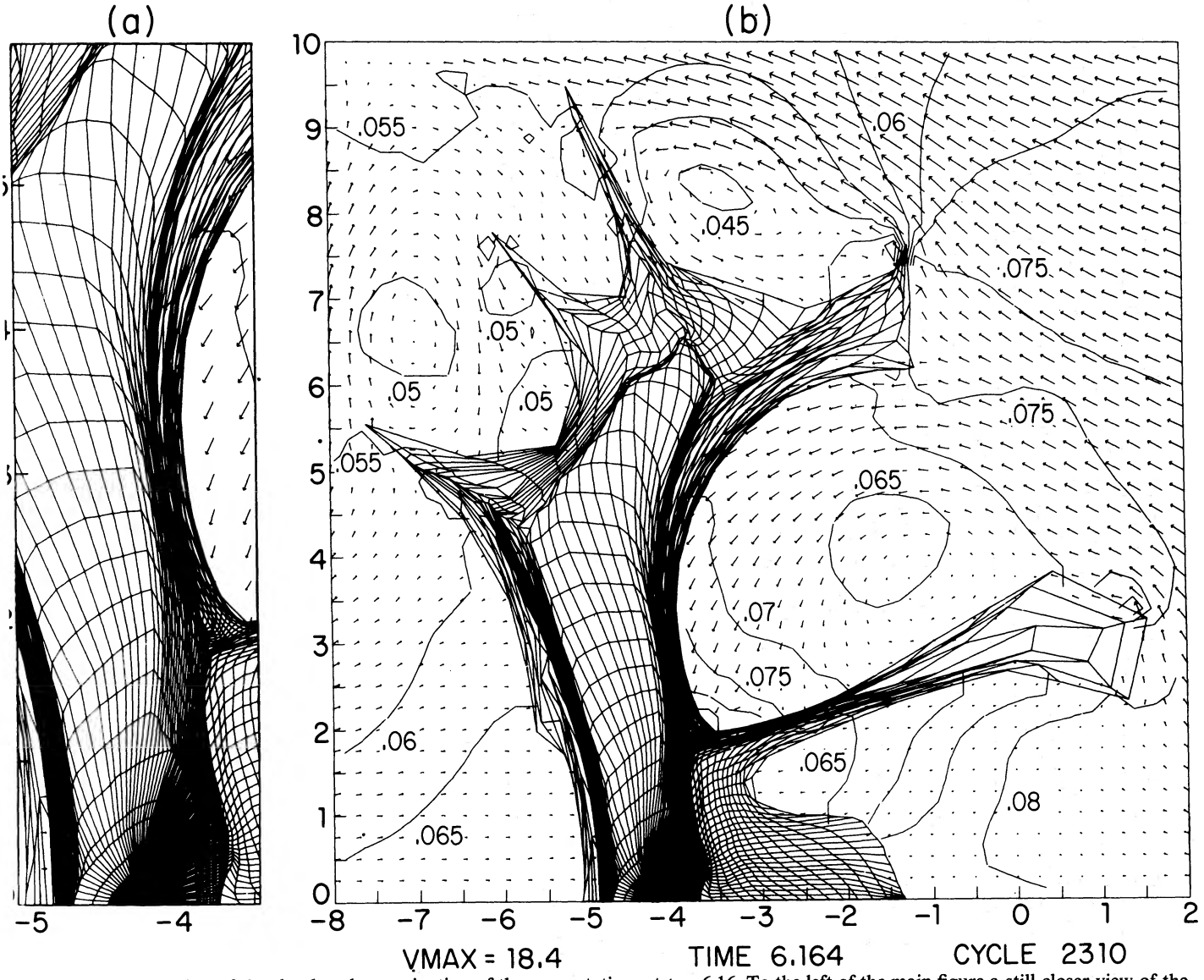

FIG. 6.—Close-up view of the cloud at the termination of the computation, at $t = 6.16$. To the left of the main figure a still closer view of the ont region of the cloud shows the shock location more clearly. Near the symmetry axis the larger Rayleigh-Taylor mode has overtaken ıe smaller one (see Fig. 5), and the dense clump contains 26.5 $M_\odot$ of material. Its gravitational energy is 90% of its thermal energy. If, for ɛample, the temperature in this clump were 23 K rather than 26 K, it would presumably collapse gravitationally to form a star or stars. As ıtercloud gas flows into the lower notch, or bay, in the cloud (between this clump and the first dense tongue), its density decreases, although s pressure decreases only very slightly. The gas in this notch has not remained on the principal post–spiral-shock adiabat (see Fig. 2) because has been trapped here while it has been repeatedly heated. This heating has come in many small jumps from little shocks. These shocks arise ıch time the lower boundary of the first dense tongue is moved slightly to allow a straightening (rezoning) of the Lagrangian grid in the tongue. he pressure of gas in this notch exceeds by about 50% that of gas of the same density outside the notch. A similar, but smaller, effect of re- ɔning has occurred in the next notch, or bay, between the two long Rayleigh-Taylor tongues. It has caused the pressure there to exceed by ɔout 15% the values for the post–spiral-shock adiabat. These errors constitute a misrepresentation of the intercloud *density* in these regions ıt not of the intercloud *pressure*. The cloud compression depends upon the intercloud boundary pressure only, and therefore is unaffected ɣ this misrepresentation. Shell densities and their locations are as follows: 250 (0, −2.5), 200 (0.5, −2), 90 (1.4, −3.5), 80 (3, 1), 75 (3.5, −4.1),) (6.3, −1.3), 50 (7.25, −1.3), 55 (6.75, −3.25), 23 (5.25, −5.3), 50 (2.25, −5.5), 70 (0, −5).

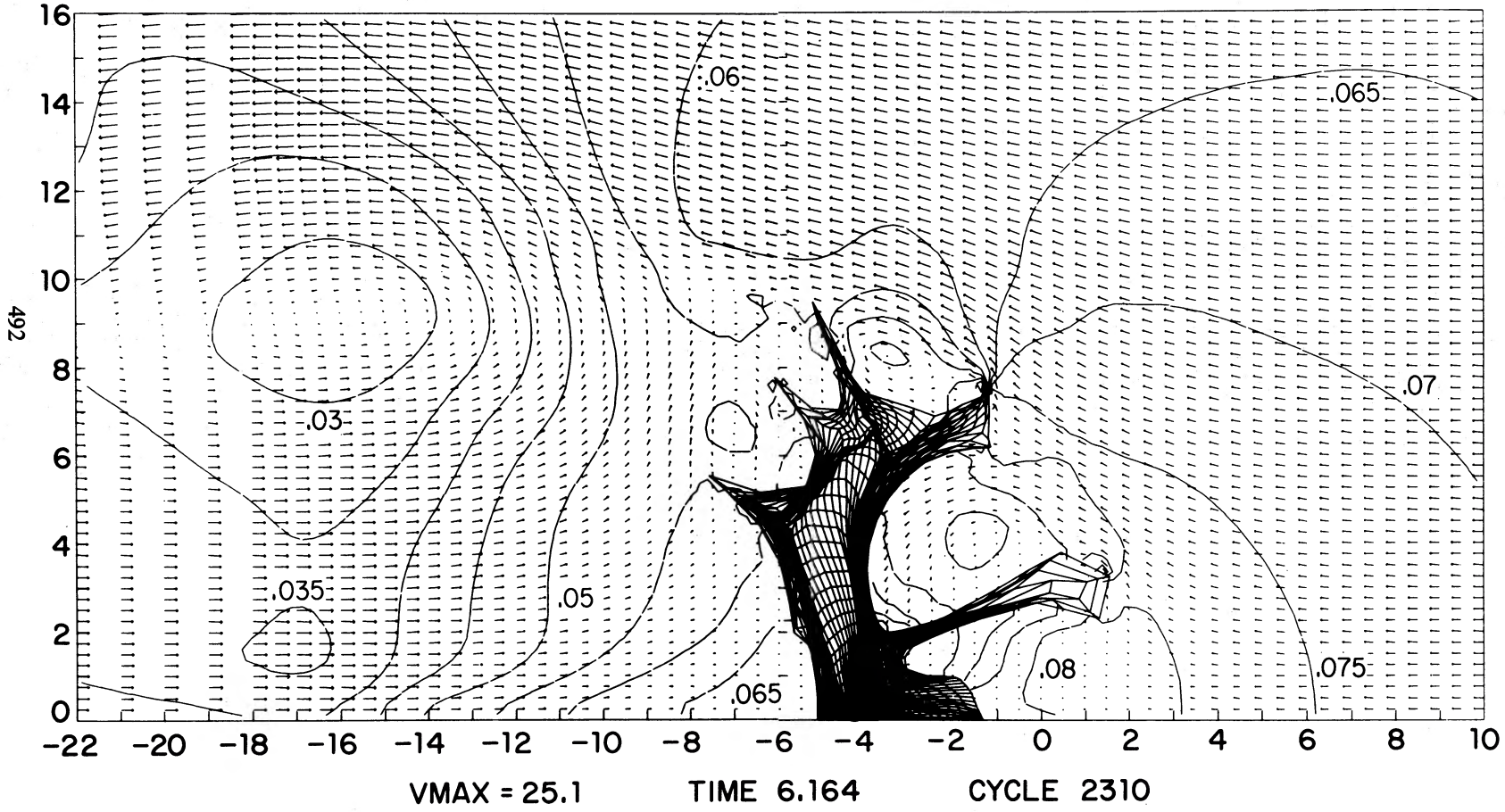

FIG. 7.—An expanded view of the flow around the cloud at the termination of the computation. Only the most interesting portion of the computational grid is shown here. Hence boundary conditions have been applied only at the lower boundary in the figure. Note particularly the very large scale of the vortex behind the cloud.

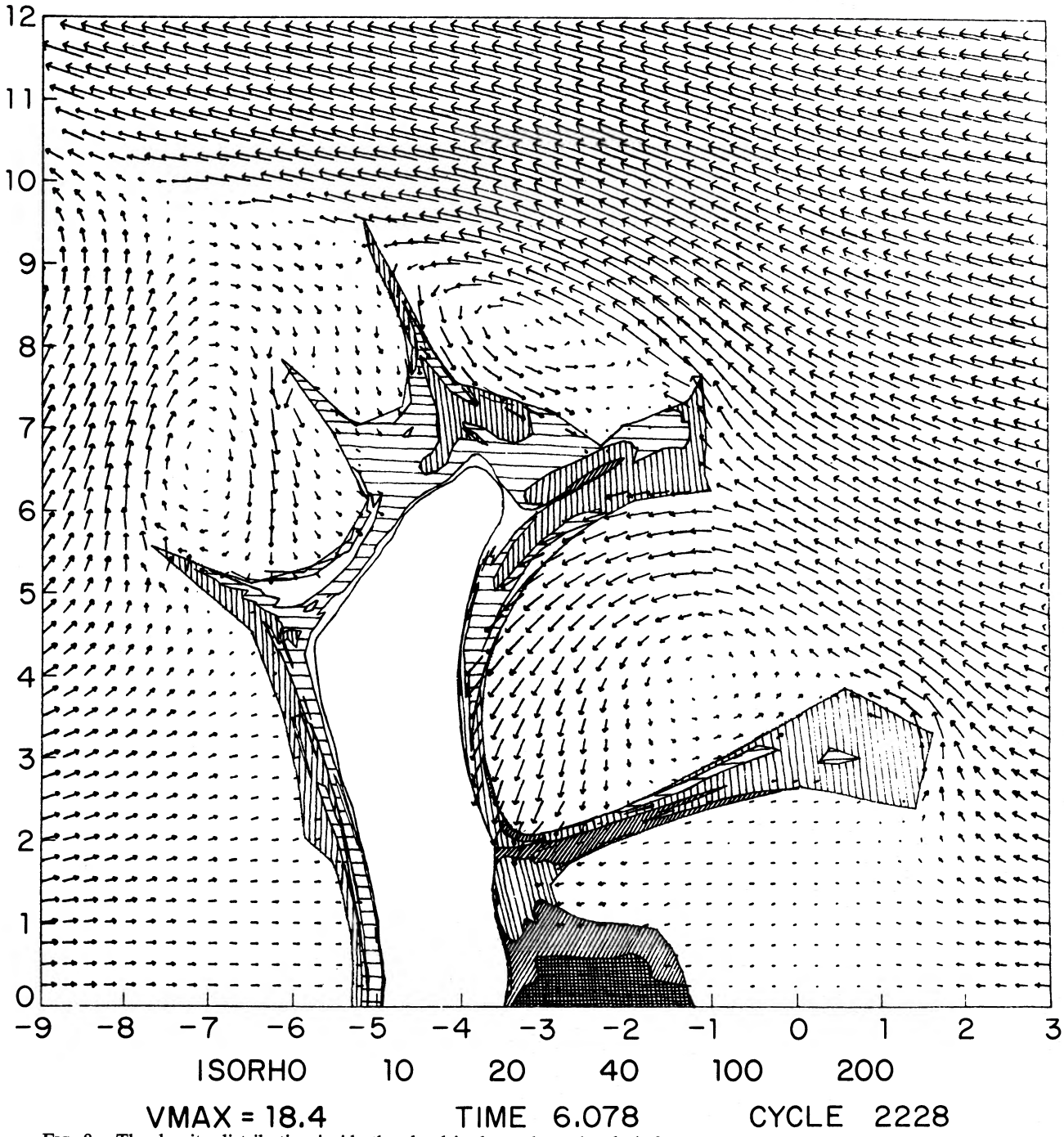

FIG. 8.—The density distribution inside the cloud is shown here shortly before the end of the computation, at $t = 6.08$. The shaded areas correspond to density contours of 20, 40, 100, and 200 atoms cm^{-3}. Also, in the unshaded area a contour at 10 atoms cm^{-3} is shown which gives the approximate location of the shock in the cloud. Within this contour essentially all the gas is undisturbed, at density 1.5 atoms cm^{-3}. The concentration of dense material in the front and back slabs is apparent. On the front, the highest densities (about 340 atoms cm^{-3}) are achieved near the symmetry axis. Relatively high densities (about 100 atoms cm^{-3}) are also obtained in the Rayleigh-Taylor tongues.

The instability near the symmetry axis must proceed more slowly than that above it because it begins in the linear regime. The growth rate is not large because most of the acceleration of the cloud material is accomplished in a shock, which is stable. Had the compression here been entirely one-dimensional, this surface would not have been unstable. However, there is a mild compression of the shocked cloud material downward toward the symmetry axis. This builds up the postshock pressure and causes the shock to accelerate. Because of this acceleration an effective gravity exists at the cloud surface which favors a buckling of that surface as it is squeezed by the motion toward the symmetry axis. Despite the slow growth rate, there is sufficient time before the front and back cloud shocks meet for the instability near the symmetry axis to develop well into the nonlinear regime. Thus there is time for modes of larger wavelength, which grow more slowly in the linear regime, to overtake those of smaller wavelength. By $t = 5.6$ (slightly after Fig. 5), the boundary near the symmetry axis is affected by essentially one unstable mode—namely, the largest possible one which can fit between the first dense tongues on either side which originally began as Kelvin-Helmholtz ripples.

As we will see in the discussion below, the speed of unstable perturbation growth near the symmetry axis plays a central role for eventual star formation. The perturbations must grow rapidly enough that dense shell material can be collected over fairly large scales, yet it must not proceed so rapidly that the collection takes place before sufficient mass has been swept up into the shell. The tuning here is not exceedingly fine. If the perturbation growth were a little too fast, gravitational forces not included in the present calculation could be invoked to slow it down and, indeed, to stop it once sufficient mass had been collected.

At selected times during the hydrodynamic calculation the gravitational potential within the cloud was computed. Although self-gravity was not included in the dynamics, these occasional potential calculations gave an idea of the importance gravity would have relative to pressure forces in a more complete treatment of the problem. Gravitational forces in the dense clump on the symmetry axis are already significant ($\frac{1}{3}$ of pressure forces) at $t = 5$ (somewhat earlier than Fig. 5). Estimates of the degree of gravitational binding of that clump can be made by a straight comparison of the gravitational and thermal energies within it or by an evaluation, using the virial theorem, of the second time derivative of its moment of inertia. At the end of the computation (Figs. 6 and 7; for density distribution see Fig. 8), both of these estimates indicate that the clump is 90 percent of the way to the brink of gravitational collapse.

This result is so close to the original goal of the calculation that, even for clouds whose masses are only moderate, we may draw the following conclusion: unless there is a tendency for immediate reexpansion of such clouds once they have been flattened, star formation can result from this implosion process. For example, gravitational binding of the clump obtained in the case computed would have been achieved had we merely chosen 23 K rather than 26 K for the temperature of the high-density branch of the cloud equation of state. Because of this near-binding of the clump at the termination of the computation, the evolution of the cloud at later times is of great importance from the point of view of star formation. If hydrodynamical considerations alone indicate that such a final cloud configuration should persist, then the addition of gravity can cause such a clump to collapse gravitationally, so that a star is born.

b) Further Evolution (Not Computed)

The cloud geometry at $t = 6.2$ (Fig. 6), when the computation stopped, suggests that the two nearly planar shocks propagating into the cloud from the front and back will collide very soon and almost simultaneously across their entire lengths. The subsequent evolution can therefore be guessed at by one-dimensional arguments, because there can be extremely little transverse motion toward or away from the symmetry axis. The shock collision causes two nearly planar reflected shocks of great strength to propagate outward in opposite directions. Between them is a slab of extremely dense, cool gas moving quite slowly (about 1 km s^{-1}) downstream. However, the details of this slab are unimportant because it does not have time to accumulate much material before it reexpands in the downstream direction.

Because of the great asymmetry of the general implosion, the shock moving into the cloud from the back does not sweep up much matter before it collides with the shock moving in from the front. Near the symmetry axis the ratio of matter swept up by the two shocks is about 1/25. The front shock is also considerably stronger than the back shock. Hence the speed of the shock reflected backward after the collision is greater than that of the shock reflected forward, and it reaches the back cloud boundary before the slab of very dense gas behind it contains much mass. From the back cloud boundary a *weak* shock is transmitted into the intercloud gas (the shock is weak because of the high intercloud sound speed) and a *strong* rarefaction wave is reflected back into the cloud. This rarefaction wave overtakes and weakens the remaining shock in the cloud, destroys the extremely dense slab at the back of the cloud, and allows the cloud material to be further accelerated in the downstream direction with at most a slight further increase in density.

In the absence of gravity, the flattened cloud would not expand much, even though the intercloud gas behind it now offers less resistance to its downstream acceleration than was offered previously by the undisturbed cloud gas. Rather than expand greatly, the cloud would accelerate more rapidly downstream. Its density would be maintained by the effective pressure pushing on the front surface. Of course, once it achieved a fair velocity in the downstream direction, the ram pressure contribution to this effective pressure would be diminished and would allow a gradual

reexpansion. It should be noted that the Rayleigh-Taylor instability of the front surface would proceed during this further acceleration, except where the surface is stabilized by the cloud's self-gravity. Consider now a case like that computed but with, say, a slightly larger initial mass or a slightly colder dense clump. The free-fall time for the clump on the symmetry axis, which, as for the case computed, would contain about 25 $M_\odot$, would be less than 4×10^6 years. In contrast, the characteristic time for the cloud acceleration and reexpansion is about 2×10^7 years.[1] Therefore, the high effective surface pressure which begins to drive the gravitational collapse of the clump would persist long enough for the collapse to be completed. The time required for star formation in such a case would then be quite short, as observations of spiral galaxies suggest it must be (Mathewson, van der Kruit, and Brouw 1972; Rots 1974)—namely, about 10^7 years.

IV. GENERALIZATION TO OTHER CASES

It is dangerous to draw general conclusions about shock-driven implosion of clouds from one computed case without strong arguments which imply that certain features of the particular calculation should also characterize other cases quite generally. This section is devoted to a presentation of such arguments. We proceed in three stages. First, we isolate features of the calculation which should generalize to a more accurate and to a truly three-dimensional treatment of the same particular problem. Second, we isolate features which should also characterize similar problems with different cloud masses. Third, we argue that certain features should persist in problems where the equation of state for the intercloud gas is more realistic.

All these arguments will focus upon phenomena which are important for star formation and will ignore many other less interesting matters. We list these phenomena briefly here:

1. The flattening of the originally spherical cloud.
2. The confinement and implosion of the back part of the cloud.
3. The marked difference in eventual unstable growth of surface ripples between regions of the surface near the symmetry axis and far from it.
4. The conglomeration of weakly amplified ripples into a single dense clump near the symmetry axis on the front of the cloud.
5. The gravitational binding of that clump.

a) The Effect of Greater Accuracy

For this discussion we ignore the first two phenomena on our list, since they are obviously well represented in the particular computation (there are, after all, some 18,000 Eulerian mesh points). The third entry is also clearly generalizable to more accurate calculations. Such calculations, with finer numerical meshes, would follow the growth of small-scale unstable modes not seen in the actual computation. Thus, down closer to the symmetry axis some small-scale ripples would have time to get help in amplification from the Kelvin-Helmholtz instability, since its growth rate is inversely proportional to the wavelength. But we are not concerned with such small-scale ripples, amplified or not, because they cannot produce a significant disruption of the cloud surface. Instead, their function is in forming a turbulent boundary layer, the details of which need not concern us.

The only entry on our list which we are at any difficulty to justify as a property which would be shared by a more accurate calculation is the fourth—that eventually the perturbation of the cloud surface near the front center is due principally to a single Rayleigh-Taylor mode whose wavelength spans the entire angular region between the first large, dense tongues which formed with prior amplification from the Kelvin-Helmholtz instability. This important result is not called into question by a limitation of the mesh spacing, since this mode has a half-wavelength of 20 Lagrange zones. It is made suspect because of its possible dependence upon the assumed cylindrical symmetry. In the problem computed, the first dense tongue is actually a cylindrical wall which acts to confine intercloud gas and to create a somewhat higher intercloud pressure below than above the wall. This pressure difference arises partly in response to the wall's downward motion and acts to decelerate it. It is the great inertia of the wall which does not allow an immediate response to and removal of this pressure difference. Nevertheless, this pressure difference is not too large, and a reduction of it in a truly three-dimensional situation should not much effect the dynamics of the cloud surface near the axis.

In a three-dimensional situation the cylindrical Rayleigh-Taylor wall of the problem computed would become several Rayleigh-Taylor tongues. It is worthwhile to point out that a Kelvin-Helmholtz instability can grow along the sides of these tongues. The growth rate for wavelengths comparable to the tongue thickness is extremely fast, so that these tongues would quickly break off. The effect upon the dynamics of the cloud surface could only be favorable for star formation, because larger Rayleigh-Taylor modes could then accumulate more material near the axis. Break-off is not important, however, for the wall configuration, for reasons which we will not go into here. In the following sections no distinction will be drawn between Rayleigh-Taylor tongues and walls, as it is likely that such a distinction has no important consequences for the dynamics near the symmetry axis, where stars are to form.

b) The Effect of Greater Cloud Mass

Here we discuss our list of phenomena in the context of a set of cases, including that computed, which differ initially only in the spherical cloud's radius, and hence its mass. We need address ourselves only to the

[1] This is the time required for the cloud to encounter its own mass of intercloud gas. Allowance has been made for the greater density of that gas in a realistic problem with cooling behind the spiral shock.

last item on the list, the gravitational binding of a dense clump of compressed cloud material located on the symmetry axis. Because all length scales inherent to the physics of the problem, such as the widths of shocks and regions of radiative cooling, have been assumed infinitesimal, the hydrodynamic equations which were solved remain invariant if all lengths and times are scaled by a common factor. However, the interplay between gravitational and pressure forces, which was not treated in the computation, does not scale in this way. As we attempt to scale the results of the hydrodynamic calculation to larger initial cloud radii and masses, the omitted gravitational forces will become relatively more important. In particular, the near-binding of the dense clump on the symmetry axis which was achieved for our cloud of 500 $M_\odot$ ensures that such clumps formed in the implosions of more massive clouds would be gravitationally bound, would collapse, and would form stars.

Had they been included in the case computed, gravitational forces would have been significant already at $t = 5 \times 10^6$ years. For the more massive clouds it seems likely that gravitational collapse and star formation may occur before the clouds are completely compressed. Then the dense shell near the symmetry axis may be perturbed chiefly by more than one Rayleigh-Taylor mode, and it is possible that stars will form in more than one region. Such clouds of more than 500 $M_\odot$ are stable in the interarm region and hence are available for implosion by the spiral shock. The implosion of these more massive clouds may give rise to the more dramatic examples of active star formation observed in the Galaxy. In such objects H II regions and new stars generally appear to be located on the outside of massive clouds of gas and dust (Liszt, private communication). This geometry is a natural feature of the shock-driven implosion discussed here (see § V), but for the very dense gas and dust we must turn to a more realistic equation of state for the intercloud gas.

c) *The Effect of Intercloud Cooling*[2]

If cooling in the intercloud gas is taken into account, the flow around the imploding cloud is altered dramatically. The spiral shock which originally collides with the cloud is followed by very rapid cooling. The shocked intercloud gas is therefore denser and produces a higher ram pressure than in the computed case, so that the total effective surface pressure applied to the cloud is nearly tripled. The density behind the front cloud shock is also nearly tripled, although the speed of that shock increases by only a factor 1.7. This increased pushing pressure can produce peak densities in the compressed outer shell of the cloud which are close to 1000 atoms cm^{-3}; and to obtain still greater densities, stronger spiral shocks can be invoked. Formation of H_2 and CO molecules with subsequent cooling to quite low temperatures will also act to increase the density in the shell still further (by a factor of about 4).

To discuss the last three phenomena on our list at the head of this section, it is necessary to see how the growth rates of instabilities change when the ram pressure on the front of the cloud is increased. In particular we would like to know how the angle, $\theta_{\min}$, changes at which long, dense tongues can be formed. The growth rate, n_{KH}, for a mode of wavenumber k of the Kelvin-Helmholtz instability of a unaccelerated fluid interface is given by (Chandrasekhar 1961)

$$n_{KH} = 1/\tau_{KH} = k v_{slip} (\rho_1 \rho_2)^{1/2}/(\rho_1 + \rho_2) .$$

Here v_{slip} is the slip velocity at the interface and ρ_1 and ρ_2 are the densities of the two fluids. We may estimate $\theta_{\min}$ by demanding that for the parameters appropriate to a disturbance of wavelength $\lambda = R/4$ on the cloud surface an angle $\theta_{\min}$ away from the symmetry axis we have

$$\alpha \tau_{KH} \approx t_{dyn} \approx R/v_{sh} ,$$

where α is a constant of order unity determined by the particular calculation. Here t_{dyn} is the dynamical time scale, R the initial cloud radius, and v_{sh} the speed of the front cloud shock. This estimate of $\theta_{\min}$ should be sufficiently good to display the correct dependence on the parameters of the problem. Now as the dynamic pressure on the front cloud surface is increased, the density there behind the cloud shock also increases. Relating this density, ρ_{sh}, to v_{sh}, we see that

$$\tau_{KH} \sim (\rho_{sh})^{1/2}/v_{slip} , \qquad t_{dyn} \sim (\rho_{sh})^{-1/2} .$$

Consequently, for a fixed angle θ, τ_{KH}/t_{dyn} is directly proportional to ρ_{sh}/v_{slip}. (Note that this ratio has no R-dependence because of the scaling property discussed in the previous section.) It is now clear that when the intercloud gas is allowed to cool, the resulting increase in shell density at the cloud surface will cause an increase in $\theta_{\min}$ if we may assume that the surface slip velocity does not increase. This is a reasonable assumption in view of the low sound speed which results from cooling in the intercloud gas.

This increase in $\theta_{\min}$ means an increase in the mass of material which can be clumped together near the symmetry axis. It is therefore favorable for star formation. Whether or not such clumping does occur, as in the computed example, depends upon the growth rate of Rayleigh-Taylor modes. When the initial surface slip velocity can be neglected, the growth rate, n_{RT}, for a Rayleigh-Taylor mode of wavenumber k in the presence of an acceleration g of the surface in the direction of the heavy fluid, with density ρ_2, is given by (Chandrasekhar 1961)

$$n_{RT} = 1/\tau_{RT} = [gk(\rho_2 - \rho_1)/(\rho_2 + \rho_1)]^{1/2} .$$

The growth rate of Rayleigh-Taylor modes is therefore unaltered by the increase in shell density ($\rho_2 \gg \rho_1$), but it is very slightly reduced (by perhaps 30%) by the increased flattening of the cloud. There is less

[2] The remarks in this section are not made completely without reference to further calculation. Some very detailed but rather inaccurate calculations of this case have been performed. In particular, they clearly imply that the first two phenomena on our list do persist in this case.

geometrical shock focusing which can act to accelerate the cloud surface. Hence we may have to wait a little while after the implosion is complete in order to make a single clump from all the material available near the axis within the angle $\theta_{\min}$. At the standard mass, star formation is still likely because of the increased shell density.

One intriguing possibility which arises when the intercloud gas cools is the formation of stars within Rayleigh-Taylor tongues which began as Kelvin-Helmholtz modes. In the case computed, these did not achieve sufficient density to be gravitationally bound. A threefold increase in density might, however, push them over the brink of instability. This possibility is merely suggested, because the *details* of these tongues may be significantly altered by the dramatic changes which must occur in the flow of the intercloud gas when it is allowed to cool.

Intercloud gas which has cooled behind a spiral shock has a sound speed of about 8 km s^{-1}. The motion of the cloud through this gas is then supersonic (about Mach 3), and a bow shock is formed. The bow shock greatly alters the gas flow around the cloud, but it does not change the general features of the flow which appear on our list; the vortex behind the cloud still develops, although with lower, subsonic velocity, and the two instabilities of the cloud surface persist. The most interesting and important new phenomenon which occurs is thermal instability in the shocked intercloud gas. The gas behind the bow shock has too high a pressure to be thermally stable in the intercloud phase. Consequently there is phase transition behind this shock which acts to lower the pressure to $p_{\max}$, the maximum stable intercloud pressure. Where the bow shock is oblique, cooling behind it proceeds very slowly and the region of phase transition may be quite far downstream. On the symmetry axis, one-dimensional calculations indicate that phase transition occurs a distance of about 2 pc behind the bow shock.

The growth rate of thermally unstable modes increases as the wavelength decreases toward a limit determined by thermal conduction (Field 1965). The wavelength of maximum growth rate is very small, so that we would expect most of the new cloud material to appear in very small bits behind the bow shock. Exactly what happens to these bits, whether they grow or are accreted by the cloud, is not clear; but the latter possibility is both appealing and likely, while the former is merely likely. It is also amusing to consider stronger spiral shocks than the case computed, which would be followed by phase transition. In this case the cloud surface is likely to be pelted with cloudlets. The detailed effects of this supersonic rain of cloudlets are impossible to compute but are most likely of no great importance so long as the fraction of the intercloud wind transformed to the cloud phase behind the spiral shock is small.

d) Speculations on the Effect of Magnetic Fields

We have argued above that those characteristics of the computed run which were essential for star formation may in fact characterize shock-driven implosions of interstellar gas clouds quite generally. However, we have consistently and purposefully ignored magnetic fields so far. Not only is the implosion with magnetic field incalculable (it is a three-dimensional problem except in one special and favorable case), but it also presents a very difficult subject for intuitive guesswork, even with the nonmagnetic calculation to guide us. As is the usual practice, we will make some remarks about the cases of the two special field orientations, parallel and perpendicular to the direction of intercloud flow, and ask the reader to perform some interpolation to the general case. We will discuss only the case of an initially uniform field with a strength which gives approximate equipartition in the shocked intercloud gas. In the case computed this field strength is 2.7 microgauss. For the large-scale context of this discussion the reader is referred to Mouschovias, Shu, and Woodward (1974).

We will consider first the case of a magnetic field parallel to the direction of relative cloud motion. In this case we would expect the flattening of the cloud to be more pronounced as a result of the impeded motion in the direction perpendicular to the field. This impediment will be stabilizing for Kelvin-Helmholtz instabilities on the front cloud surface. Also, the growth of Rayleigh-Taylor instabilities of short wavelength will be slowed. For the largest modes of interest, the growth rate is reduced by a factor of about 4. Therefore, these instabilities will not act so effectively to gather the dense material together into tongues and clumps. At best we would have to allow the Rayleigh-Taylor instability to collect matter for a substantial time after the implosion is complete in order to obtain bound gas clumps. Several million years are available for this process before the cloud reexpands a great deal. The compression of the gas inward into a dense shell will not be impeded by the magnetic field, but eventual star formation will be less likely in this case. In addition, the resistance of the field lines to bending will oppose the development of the Kelvin-Helmholtz instability at the sides of the cloud. Thus in general the cloud implosion will be flatter and smoother in this case.

For the magnetic field oriented perpendicular to the direction of relative motion the situation is more complex. Consider first the sides of the cloud. Where the field lines are parallel to the cloud surface, the Kelvin-Helmholtz instability is unimpeded but the cloud compression is reduced by the opposing magnetic pressure. Where the field lines are perpendicular to the cloud surface, they act to inhibit the development of the Kelvin-Helmholtz instability but they do not restrict the cloud compression. Therefore, a cross section of the cloud made perpendicular to the direction of its relative motion will become increasingly elliptical in shape as the implosion proceeds. Also, the sides of greater curvature would be perturbed by Kelvin-Helmholtz ripples.

Now consider the situation at the front of the cloud. The growth of perturbations in the direction along the field lines is impeded by the tension of the lines

of force. For an equipartition field strength (2.7 microgauss) all wavelengths of interest are stabilized. The most interesting modes, the larger ones, are unstable if the field strength is lowered to about half this value. In the orthogonal direction the instability proceeds unimpeded by the magnetic field. Without the Rayleigh-Taylor instability, the resistance of the magnetic pressure would make high densities in the compressed shell impossible to obtain, and would make eventual star formation in the manner we have discussed extremely unlikely.[3] However, if the field is sufficiently weak that perturbations of fairly large wavelength (about 4 pc for a standard cloud) can grow well into the nonlinear regime, fairly high densities may be achieved, and star formation may proceed more or less as in the computed example. For this to occur the field strength would have to be significantly less than 1 microgauss.

In summary, star formation along the lines discussed for the computed example is more likely to occur if the magnetic field is either relatively weak or relatively well oriented, with the field direction not too different from the direction of cloud motion relative to the intercloud gas. The results of detailed calculations are needed to draw quantitative conclusions, but the problem is three-dimensional and we must not expect such calculations to appear in the near future.

V. OBSERVATIONAL IMPLICATIONS

Although detailed comparisons of the computed example with specific objects will be reserved for a later paper, we will give a brief summary here of the general features of the cloud implosion mechanism which bear on observations of dense interstellar clouds. Those observations quite naturally tend to favor the more massive and more exotic objects, which would require the case computed here to be scaled up considerably in mass, by perhaps a factor 10 or 20. The features of the model most important for observations are as follows:

1. Stars are formed in small high-density regions within much more massive and extended clouds.
2. The extended region of dense cloud gas produced, which is visible in CO emission, has a general slab geometry, so that a straightforward mass estimate can easily yield far too large a number.
3. Young stars and H II regions appear to be located on the outsides of dense gas clouds.
4. The newly formed stars and the associated dense gas have systematic noncircular velocities which depend upon their location in the Galaxy.
5. Dense gas which originally surrounds the newly formed stars but which cannot collapse gravitationally is eventually swept away by external forces.
6. Ordered motions not associated with gravitational collapse are set up in the dense cloud material which result in supersonic broadening of CO lines.

a) Cloud Context for Star Formation

The first and most important consequence of the cloud implosion model is that stars form from this mechanism in very restricted regions within much more massive, extended clouds of gas. In the computed example the mass of the cloud is 20 times that of the gas which comes close to gravitational collapse (that is, the dense clump on the symmetry axis). The linear dimension of the cloud is 15 pc, while that of the dense clump is 2 pc. Observed from nearly any angle, this cloud would appear very large, although perhaps elongated in the direction perpendicular to the galactic plane.

b) Mass Estimate

With cooling included in the intercloud gas, sufficient densities are certainly obtained during the cloud implosion in order to excite CO. If the excitation is primarily radiative (for densities below about 10^5 atoms cm^{-3}), as the recent detailed work of Leung suggests (private communication), CO may be observed where the density exceeds about 100 atoms cm^{-3}. If the imploded cloud were observed in CO and its mass were deduced from a minimum excitation density and a spherical volume corresponding to its angular extent, a tremendous overestimate would result. Leung and Liszt (1976) have demonstrated that differing excitation mechanisms for ^{12}CO and ^{13}CO result when ^{12}CO is radiatively excited. This situation allows theoretical line strength ratios between the two molecules to be much smaller than their cosmic abundance ratio, even for ^{12}CO optical depths of order unity. Therefore, CO sources may not be optically thick, and a slab geometry is entirely consistent with the CO observations when a detailed calculation of radiative transfer is used to interpret the data.

Without some justification such as that provided by the cloud implosion mechanism, the introduction of a slab model for dense interstellar clouds would be ad hoc. Therefore, it is not surprising that current thought about these objects tends to assume, either explicitly or implicitly, a roughly spherical geometry. However, this picture presents several problems for theoreticians. First among these is the value of the mass deduced, which is typically between 10^5 and 10^6 $M_\odot$. Spherical clouds, without rotation or magnetic field, which are located within spiral arms must

[3] For strong fields of this orientation it seems that a cloud would approach its eventual downstream equilibrium state quite smoothly. If the cloud is sufficiently massive, this state is a pancake perpendicular to the field direction. If it is still more massive, no such state is possible at the new spiral arm pressure, and gravitational collapse must ensue. However, this is a rather different sequence of events than we have been discussing with reference to the computed example. The sequence is meaningful in this case because the suppression of surface instabilities by the magnetic field does not permit mass loss from the cloud into dense Rayleigh-Taylor tongues which break off or into spray from "breaking" Kelvin-Helmholtz waves. We should also note that the time required for such a transverse implosion is likely to exceed that for the computed case by a factor of 2 or 3. This would increase the spatial separation between a spiral shock and the stars whose formation it initiates, and hence would give rise to a broader band of spiral tracers (H II regions and OB associations).

collapse gravitationally if their masses exceed about 200 $M_\odot$ (see Shu *et al.* 1972). It is therefore difficult to understand how 10^5 or 10^6 $M_\odot$ of gas could be brought together to form one cloud without all the component pieces collapsing gravitationally long before the collection process could be completed.

This difficulty vanishes when a slab geometry for the dense clouds is assumed. Deduced masses for the clouds are then drastically reduced, so that they fall in the stable range for clouds *in the interarm region*. A stable spherical cloud, with no rotation or magnetic field, may contain up to about 3000 $M_\odot$ in this low-pressure region (Shu *et al.* 1972). The large spatial extents observed for dark clouds in spiral arms (up to 20 pc) can then be understood as a result of the very low density of the normal cloud phase *between* spiral arms. H II regions containing 100 $M_\odot$ can be produced by normal interstellar clouds of about 2000 $M_\odot$, which would have diameters of about 50 pc upon meeting a spiral shock. In the computed example the cloud dimension transverse to the flow direction (parallel to the spiral arm shock) was reduced by a factor of 2 during the implosion. Cooling in the intercloud gas, which was not included in the case computed, would increase the ram pressure on the front of the cloud without changing the kinetic pressure on the side of the cloud. Therefore, a more realistic treatment would yield a smaller transverse compression, hence a greater flattening, of the cloud. Consequently, a cloud of 2000 $M_\odot$ should have a final linear dimension greater than 30 pc. Thus it is reasonable to expect an extended CO source 20 pc in dimension to be associated with the birth of 100 $M_\odot$ of stars.

c) *Apparent Location of* H II *Regions*

The assumption of a roughly spherical shape for dense gas clouds results in another difficulty still more perplexing than the first. This is the apparent location of newly formed stars on the outsides of very dense, massive clouds and not at their centers (Liszt, private communication). The situation is graphically presented, for the case of Orion, in Figure 2 of Zuckerman and Palmer (1974). This figure should be contrasted with Figure 8 of this article. If the cloud shape is roughly spherical, nearly any theory of gravitational collapse would produce new stars at the dark cloud center. H II regions buried from view (optically) within the cloud have been searched for but not found. Therefore, the picture which the observations suggest is perplexing.

If, however, the CO emission arises in a thin slab rather than a sphere, it is no longer surprising that the H II region is visible. For massive clouds, stars can form in the dense slab while it is still bounded on one side by undisturbed cloud material. An H II region formed at this time would be visible from the front only (from the right in Fig. 8). The great pressure exerted by the H II region would strengthen the nearby shock and cause it to compress undisturbed cloud material to extremely high density. This region behind the shock would obscure the H II region if the cloud were viewed from the back. Molecules which require very high gas densities for their formation and excitation could be observed in this shock region, which might therefore be easily mistaken for the center of a dense collapsing gas cloud. It is tempting, for example, to think of the very dense molecular cloud right behind the Orion Trapezium in these terms.

d) *Relation to Spiral Wave Geometry*

The geometry of spiral wave flow in the Galaxy implies that the clouds, the young stars, and the associated H II regions should, on the average, show a component of noncircular velocity which is directed partly outward from the center of the Galaxy and partly opposite to the direction of the average circular rotation. The spiral-wave flow geometry also tells us on which side of a *large* dark cloud, toward or away from us, an H II region should appear to be located. It should appear to be on that side which faces radially outward from the galactic center. For small clouds, H II regions would be visible from either side. For those H II regions which are visible optically, we would also expect to see tongues of dense gas projecting toward us in adjacent areas on the sky. These tongues of gas might also be lit up by the newly formed stars and appear as reflection nebulae.

e) *Removal of Gas Which Does Not Form Stars*

In a recent review article Strom, Strom, and Grasdalen (1975) have pointed out a difficulty which arises from present ideas about star formation in massive dark clouds. Stars and clusters are observed outside such clouds, so we are led to the conclusion that the cloud material is somehow dispersed after the stars have formed. This dispersal is difficult to accomplish using only those forces which come immediately to mind. Stellar winds and expanding H II regions can push away only a small fraction of the total cloud mass. To disperse the entire cloud, more speculative processes must be invoked which operate over longer time scales—supernova explosions, cloud collisions, and galactic differential rotation.

The cloud implosion model presented here manages to resolve the above difficulty easily. The cloud is eventually swept away, in about 2×10^7 years, by the same external force which helped to squeeze it together, the ram pressure of the intercloud gas flow. As the cloud is swept away, it gradually reexpands and effectively disappears. The cloud does not disappear without a trace, of course, and its remains should be located downstream in the form of normal, diffuse interstellar cloud material. The eventual velocity of this material relative to the newly formed stars is expected to be about 20 km s^{-1}. Since the direction of this velocity is also predicted, at least on the average, the model tells us where we would expect to observe the remaining cloud material. This straightforward resolution of a long-standing difficulty was made possible because the implosion model allows us to make use of a vast external energy source to sweep the cloud material away—namely, the energy of the

galactic shock, which is in turn derived from the release of gravitational potential energy to the interstellar gas as it falls into the potential well of a spiral arm.

f) *Broadening of* CO *Lines*

A mysterious feature of CO observations of dark clouds has been the supersonic broadening of the lines or of their velocity components. To explain this broadening, supersonic turbulence or gravitational collapse has been proposed. Supersonic turbulence is objectionable because it dissipates so rapidly that a vast and continuous energy source is required to maintain it. Objections have also been raised to gravitational collapse on the grounds that it may predict an unreasonable rate of star formation in the Galaxy (Zuckerman and Palmer 1974). In the front dense shell in the computed example, systematic velocity differences of 2 to 2.5 km s^{-1} (Mach 4.3 to 5.4) are produced. These are the combined result of shock acceleration and Rayleigh-Taylor instability. Thus we can obtain supersonic velocity broadening of CO lines without turbulence and without collapse (that is, at least without collapse of all the material observed). The ordered motion we obtain in the implosion model by squeezing the cloud gas is similar *observationally* to that which we might obtain by pulling on the cloud gas in a general gravitational collapse of the entire cloud. But the slab geometry which results in the former situation ensures that only a small fraction, if any, of the gas observed will end up in stellar form. Thus the classic objection to the collapse model is avoided.

We will close this section by mentioning that weak observational constraints have been placed upon the time required for star formation initiated by a spiral wave shock. Mathewson, van der Kruit, and Brouw (1972) and Rots (1974) have given estimates of order 10^7 years for this time, deduced from their observations of M51 and M81, respectively. An attractive feature of the mechanism discussed here is that it can easily produce stars within this rather short time scale.

VI. CONCLUSIONS

The computed example presented here demonstrates that star formation can be initiated by large-scale spiral shocks located along the arms of spiral galaxies. If relatively dense clouds exist in pressure equilibrium with a more diffuse intercloud medium in the region between spiral arms, the clouds are imploded upon passing through a spiral shock. The implosion is driven by the combined effective pressures of the shocked intercloud gas and the motion of that gas relative to the cloud. Without magnetic field, this implosion is both asymmetrical and unstable. The clouds are flattened generally, and their surfaces are greatly disrupted by instabilities. Consequently these clouds do not tend to collapse as a whole under the action of their strengthened self-gravity. They may even lose mass as dense tongues of material projecting outward from their surfaces break off or as waves along their sides are amplified and break, sending a spray of dense material off into the surrounding flow.

Despite all this asymmetry and possible mass loss, gravitational collapse and star formation may occur. Although the original spherical symmetry is completely lost and matter motions within the cloud are not focused into a convergence upon the cloud center, the instabilities themselves focus matter motions on smaller scales and collect cloud material together in clumps which can eventually collapse. In this process the mutual interaction of the Kelvin-Helmholtz and Rayleigh-Taylor instabilities plays a critical role, and matter accumulation is most favorable near the front center of the cloud surface, where only the latter instability has a chance to act.

The collection of cloud matter by the surface instabilities could not ultimately result in star formation were it not for the transient nature of the flow. That is, the entire implosion takes place before the intercloud gas has a chance to accelerate the cloud center of mass to any great extent. Therefore, throughout the implosion the effective pressure at the cloud surface is greatly enhanced by the ram pressure of the intercloud gas motion. This high effective surface pressure yields greater densities in the shocked cloud gas than would be attained during a gradual implosion in which the surface pressure climbed slowly to its final value in the spiral arm (such gradual implosions would occur where there are no spiral shocks along a spiral arm, such as near the region of corotation with the spiral pattern). These high pressures and densities are an essential element of the mechanism of star formation discussed here. They result from the sudden, asymmetrical forcing of the cloud implosion which the spiral shock produces, and they make gravitational collapse of subregions of the cloud possible.

Previous calculations which attempted to produce gravitational collapse of diffuse interstellar gas have relied upon very special symmetries to achieve favorable results. In the work of Stein, McCray, and Schwarz (1972), a perfectly spherical implosion is assumed and a very strong geometrical shock focusing is exploited to obtain gravitational collapse. In the work of Stone (1970), two clouds of exactly equal mass collide precisely head on. The present work is suspect in this regard because of the perfectly spherical shape of the unshocked cloud. However, this symmetry is immediately destroyed. The asymmetry of the implosion, which prevents overall cloud collapse, is nevertheless advantageous for collapse of subregions of the cloud. The surface instabilities which are disastrous for spherical implosions then work favorably to collect dense gas into clumps which may become gravitationally bound. The present model is not invulnerable, of course; a large-scale, large-amplitude perturbation of the front center surface of the initial cloud might have very unfortunate effects. The magnetic field also has been ignored. However, it is hardly necessary that *every* cloud of standard mass or greater should produce stars upon entering a spiral arm. The general observational implications of the model are so

convenient (CO observations are made easier for theoreticians to live with) and the hydrodynamical features of the model are so reasonable (the results are sufficiently contorted and messy to correspond to the real world) that the cloud implosion mechanism described here provides a very appealing explanation for the narrow lanes of bright, young stars which trace the spiral arms of galaxies.

I am pleased to acknowledge the helpful discussions I have had with G. B. Field, F. H. Shu, C. F. McKee, and W. F. Noh. I am also most grateful for the use of the computer facilities of the Lawrence Livermore Laboratory and for the helpful cooperation of the CEL code group there. This work was supported in part by the National Science Foundation under research grant GP-36194X.

REFERENCES

Chandrasekhar, S. 1961, *Hydrodynamic and Hydromagnetic Stability* (Oxford: Oxford University Press).
Field, G. B. 1965, *Ap. J.*, **142**, 531.
Field, G. B., Goldsmith, D. W., and Habing, H. J. 1969, *Ap. J.* (*Letters*), **155**, L149.
Leung, C. M., and Liszt, H. S. 1976, to be submitted to *Ap. J.*
Lin, C. C., Yuan, C., and Shu, F. H. 1969, *Ap. J.* **155**, 721.
Mathewson, D. S., van der Kruit, P. C., and Brouw, W. N. 1972, *Astr. and Ap.*, **17**, 468.
Mouschovias, T. Ch., Shu, F. H., and Woodward, P. R. 1974, *Astr. and Ap.*, **33**, 73.
Noh, W. F. 1964, in *Methods in Computational Physics*, Vol. 3, ed. B. Alder, Fernbach, and Rotenberg (New York: Academic Press).
Roberts, W. W. 1969, *Ap. J.*, **158**, 123.
Rots, A. H. 1974, unpublished thesis, University of Groningen, The Netherlands.
Shu, F. H., Milione, V., Gebel, W., Yuan, C., Goldsmith, D. W., and Roberts, W. W. 1972, *Ap. J.*, **173**, 557.
Shu, F. H., Milione, V., and Roberts, W. W. 1973, *Ap. J.*, **183**, 819.
Spitzer, L. 1968, *Diffuse Matter in Space* (New York: Interscience).
Spitzer, L., and Scott, E. H. 1969, *Ap. J.*, **158**, 161.
Stein, R. F., McCray, R. A., and Schwarz, J. 1972, *Ap. J.* (*Letters*), **177**, L125.
Stone, M. E. 1970, *Ap. J.*, **159**, 293.
Strom, S. E., Strom, K. M., and Grasdalen, G. L. 1975, preprint.
Woodward, P. R. 1975, *Ap. J.*, **195**, 61.
Zel'dovich, Ya. B., and Pikel'ner, S. B. 1969, *Zh. Eksper. Teoret. Fiz.*, **56**, 310.
Zuckerman, B., and Palmer, P. 1974, *Ann. Rev. Astr. and Ap.*, **12**, 279.

PAUL R. WOODWARD: Sterrewacht, Huygens Laboratorium, Wassenaarseweg 78, Leiden 2405, The Netherlands